APPLICATION OF FREQUENCY-DEPENDENT AVO INVERSION TO HYDROCARBON DETECTION

SHUANGQUAN CHEN[1,2,3], XIANG-YANG LI[1,2,3] and XIAOYANG WU[3]

[1] *State Key Laboratory of Petroleum Resources and Prospecting, China University of Petroleum, Beijing 102249, P.R. China. stonecsq@126.com*
[2] *CNPC Key Laboratory of Geophysical Prospecting, China University of Petroleum, Beijing 102249, P.R. China.*
[3] *British Geological Survey, Murchison House, West Mains Road, Edinburgh EH9 3LA, U.K.*

(Received September 30, 2013; revised version accepted April 9, 2014)

ABSTRACT

Chen, S.-Q., Li, X.-Y. and Wu, X.-Y., 2014. Application of frequency-dependent AVO inversion to hydrocarbon detection. *Journal of Seismic Exploration*, 23: 241-264.

Seismic wave dispersion results mainly from fluid flow in a heterogeneous porous medium, and reflectivity at the interface of a dispersive medium is frequency-dependent. In theoretical rock physics, reflectivity can be expressed as a function of velocities which are frequency-dependent, and the expressions of prestack Zoeppritz equations are also frequency-dependent. In this paper, we develop a frequency-dependent AVO inversion (FDAI) method that is based entirely on the frequency-dependent seismic response attributes of prestack seismic data, and apply it to a hydrocarbon detection case study. Analysis of elastic, frequency-dependent media using synthetic methods demonstrates improved hydrocarbon detection by FDAI compared to conventional AVO inversion. Application to a real field seismic dataset indicates that seismic wave dispersion resulting from the hydrocarbon inclusions can be detected using the frequency-dependent inversion method. In particular, for reservoir characterization and hydrocarbon detection, dispersion characteristics due to wave-induced fluid flow in the porous reservoir can be interpreted advantageously using the FDAI method.

KEY WORDS: frequency-dependent, AVO inversion, dispersion, hydrocarbon detecting, time-frequency decomposition.

0963-0651/14/$5.00

INTRODUCTION

In seismic exploration for petroleum, the main tool for hydrocarbon detection is presently fluid substitution modelling (Gassmann, 1956), in seismic inversion and interpretation. The main consideration is that seismic records contain information on the fluids in the porous media through which the seismic waves propagate. Seismic characteristics of fluid-saturated rocks such as velocity dispersion can be frequency-dependent (Chapman et al., 2006). Seismic wave velocity dispersion is related to the concept of fluid flow (Batzle et al., 2006), as the driving mechanism for dispersion is believed to be the wave-induced exchange of fluid between different regions within the porous rock.

The attenuation of a seismic wave refers to the exponential decrease of wave amplitude, and the variation of wave phase with distance; dispersion is the variation of seismic wave velocity with frequency during propagation. Velocity dispersion in the seismic frequency range is also observed in low-frequency measurements in the laboratory (Batzle et al., 2001). Seismic wave attenuation and dispersion resulting from wave-induced fluid flow between pores are particularly relevant to exploration geophysics, because the fluid-related dissipation of energy in the hydrocarbon reservoir can be inverted from recorded seismic data (Li and Zhang, 2011). This highly interesting topic is gaining increasing attention (Goloshubin and Korneev, 2000; Castagna et al.,, 2003; Korneev et al., 2004; Chapman et al., 2006). Biot's theory of poroelastic wave propagation (Biot, 1956a, 1956b, 1962) underestimates velocity dispersion and attenuation (Mochizuki, 1982; Dvorkin et al., 1995; Parra, 2000; Arntsen and Carcione, 2001; Ebrom, 2004; Pride et al., 2004). The combined effects of mesoscopic-scale inhomogeneities, and energy transfer between wave modes, indicate that high attenuation and velocity dispersion can be explained as a mesoscopic loss mechanism, as proposed first by White (1975, 1986) and White et al. (1975), where the mesoscopic scale is much larger than the grain size, but much smaller than the wavelength.

After studying Biot loss, scattering, and mesoscopic-flow loss for 1D thinly layered poroelastic media, Gurevich et al. (1997) confirmed that the attenuation peak for mesoscopic-loss occurs at a lower frequency than that for scattering attenuation. Shapiro and Müller (1999) concluded that frequency-dependent P-wave attenuation can be observed in the seismic frequency range through a study of the fluid-mobility effect on P-wave attenuation for thin partially saturated media, and Johnson (2001) proposed a new White's model for pores of arbitrary shape. Müller and Gurevich (2004) performed numerical experiments on random and periodic media with patchy saturated media (i.e., containing both gas and water inclusions) and showed that the attenuation peak occurs in the seismic band at 80% water saturation. Carcione and Picotti (2006) studied velocity dispersion and attenuation for thinly layered, partially saturated media and found that the attenuation peak for patchy

saturation can occur in the seismic frequency range. For the anisotropic case, Chapman (2003) established a link between seismic wave behaviour and the scale length of fractures, for a single set of fractures. Later, Chapman et al. (2006) extended the analysis of seismic wave dispersion modeling in fractured media to two sets of fractures, with different scale lengths and orientations. Theoretical investigations (Jakobsen and Chapman, 2009) unifying global flow and squirt flow of fluid in porous and crack media were also carried out for an understanding of this frequency-dependence.

As mentioned above, attenuation and velocity dispersion can have a substantial influence on seismic data in hydrocarbon-saturated zones. Researchers have made some significant attempts at frequency-dependent AVO analyses (Yoo and Gibson, 2005; Marmalyevsky and Roganov, 2006; Chapman et al., 2006; Odebeatu et al., 2006; Liu et al., 2006). Chapman et al., (2006) performed a theoretical study of reflections from the interface between a layer exhibiting fluid-related dispersion and an elastic overburden, and showed that in such a case the AVO response was frequency- dependent. Using a patchy-saturated model, Ren et al. (2008, 2009) studied reflection coefficient variations with frequency, including magnitude and phase angle, for P-waves at normal incidence on a dispersive medium. Based on analytic equations and numerical modeling, Liu et al. (2011) investigated the AVO characteristics of frequency-dependent amplitude versus incident angle at an interface between a nondispersive medium and a partly-saturated dispersive medium. Innanen (2011) proposed a Q-value estimation AVF/AVA method by studying the series expansions of absorptive reflection coefficients.

The theoretical analysis was extended to an inversion of seismic prestack data, introducing a frequency-dependent AVO inversion concept aimed at allowing a quantitative measure of dispersion to be derived from prestack data. Wilson et al. (2009) and Wu et al. (2010, 2012) proposed an inversion scheme involving frequency-dependent prestack inversion to analyze the frequency effect of velocity dispersion on reflection coefficients. They tested the method using synthetic seismic data and real field seismic data, and indicated that the inversion processing workflow is feasible. Xu et al. (2011) used the frequency-dependent seismic reflectivity of poststack seismic data to predict a gas reservoir. Zhang et al. (2011) inverted the dispersion-dependent attributes of P-wave velocity and gradient by rearranging Shuey's equation (Shuey, 1985) to add the frequency content directly. Chen et al. (2012) used a physical model dataset and verified the theoretical frequency characteristics for a Class I AVO reservoir.

This paper is an extension of the frequency-dependent AVO inversion study. We try to invert the characteristics of frequency-dependent amplitude versus incident angle at an interface between non-dispersive and dispersive media, aiming to provide enlightenment for a frequency-dependent AVO

inversion (FDAI) method for hydrocarbon detection in a real field reservoir. We have reviewed the frequency-dependent AVO expressions and developed a prestack inversion method for P-wave velocity dispersion from seismic gathers. The method uses time-frequency decomposition information from prestack seismic gathers to invert the seismic wave velocity dispersion component related to hydrocarbon saturation. In order to provide accurate attribution, true seismic amplitude variation with offset must be maintained in each CDP gather, and the influence of NMO stretch must be suppressed in seismic data processing.

Our workflow is as follows: first, we review the wave-induced seismic frequency dispersion and the frequency-dependent amplitude versus offset and compare the differences between elastic and frequency-dependent synthetic data. We then derive the frequency-dependent AVO equation and introduce a FDAI method to obtain the hydrocarbon response in terms of frequency-dependent characteristics, based on the study of frequency-dependent amplitude versus offset (AVO), or incident angle (AVA), at an interface with a dispersive medium. Finally, we apply the FDAI method to a real field seismic dataset from a hydrocarbon-bearing reservoir and certify the frequency-dependent dispersion characteristics.

FREQUENCY-DEPENDENT AVO AND INVERSION METHOD

Frequency-dependent AVO

In the case of reflection from a single interface, Gassmann's theory predicts that fluid substitution in one of the layers will change the impedance contrast and therefore the amplitude of the reflection (Gassmann 1951). This effect is independent of frequency. Reflections from a thin layer are typically composite events, which result from the superposition of top and bottom reflections. In this case, fluid substitution will also change the traveltime within the thin layer, and this alters the interference between the two reflections. This effect does lead to a change in frequency, so we expect fluid substitution to be intrinsically frequency-dependent in multiple thin layers.

Based on the squirt-flow mechanism, Chapman (2003) has presented an equivalent medium theory for fracture modeling, which encompasses both the Thomsen low frequency limit and Hudson high frequency limit to derive the seismic wave dispersion response. He argues that by introducing larger scale heterogeneity (centimetre to metre scale), the transition frequency shifts from a high frequency band into the seismic band. The modelling assumes that low frequencies correspond to the case of pressure equalization, where fluid has time to move to relieve local pressure gradients within the time period of a seismic wave. In contrast, at high frequencies the fluid does not have time to move and the pressure gradients persist. Between these two cases, velocity dispersion and

associated attenuation occur as the elastic properties move between the compliant low-frequency case and the stiffer high-frequency case. The mathematical procedure for calculating the frequency-dependent constants is outlined in Chapman et al. (2006).

Chapman et al. (2006) have presented a modelling framework which accounts for fluid-sensitive dispersion and attenuation. In this modelling, the introduction of gas results in a marked increase in attenuation, and associated dispersion. Attenuation leads to a loss of high frequencies during propagation. The existence of strong dispersion in a hydrocarbon-saturated layer leads to frequency dependence of the impedance contrast at the interface and so makes the reflection coefficient frequency-dependent. This tends to shift the reflections to higher or lower frequencies quite markedly compared to the background trend, with the direction of the shift depending on the AVO class of the reflection. This reflection response does not depend on the thickness of the layer and is the main focus of our study. Chapman et al. (2006) demonstrated that the spectral response of the tuning and dispersion effects were often comparable in magnitude, and argued that both have to be taken into account to interpret seismic data properly. Odebeatu et al. (2006) introduced a technique for spectral balancing and differencing of frequency volumes, which shows the spectral anomalies particularly clearly.

Fig. 1 shows an example of velocity and attenuation variation with frequency. Fig. 1a shows a decrease in P-wave velocity from high frequency to low frequency for both gas and water saturations in a sandstone. The parameters of the sandstone are V_P = 2790 m/s, V_S = 1463 m/s, and ρ = 2.08 g/cm^3 with water saturation, ρ = 2.06 g/cm^3 with gas saturation, and porosity = 30%. The bulk moduli of gas and water are taken as 400 Mpa and 2000 Mpa, respectively. The reference frequency is 10 Hz, crack density is 0.1, and time-scale value 2 x 10^{-5} s. The Gassmann effect is shown by the decreasing P-wave velocity when gas replaces water. The P-wave velocity with gas saturation shows a larger difference between high and low frequency, and higher attenuation than for water saturation, which indicates that gas saturation can lead to abnormally high attenuation. Fig. 1b shows that there is no Gassmann effect for the S-wave case, because at low frequency the shear-modulus is decoupled from the saturating fluid. S-wave attenuation is very small for gas saturation compared to the P-wave case.

Inversion methodology

The FDAI method is based on the simplified AVO inversion equation using prestack seismic gathers (Wilson et al., 2009). Wilson et al., (2009) use a heuristic approximation from the simplified AVO equation of Smith and Gidlow (1987). Here, we derive the AVO equation from frequency-dependent

reflectivity. As the dispersion information is related to seismic wave velocities, we should set up an inversion method to quantify the variation of wave velocities using the pre-stack seismic data. Using Aki and Richards' (1980) linearization AVO equations, Smith and Gidlow (1987) proposed a two-term AVO approximation, in which the reflection coefficient R is a function of P- and S-wave seismic wave velocity. In the Appendix, where we rewrite the frequency-dependent AVO matrix, an analogous equation is proposed for the dispersion inversion using the prestack gather. Considering the frequency-

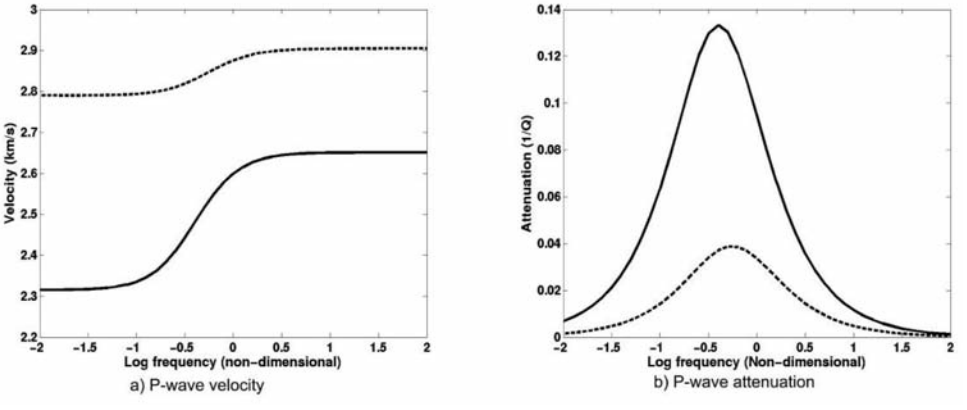

Fig. 1a. Predicted P-velocity and attenuation as a function of non-dimensional frequency $\omega\tau$ under gas and water saturation (solid line: gas, dashed line: water) (Chapman et al., 2006).

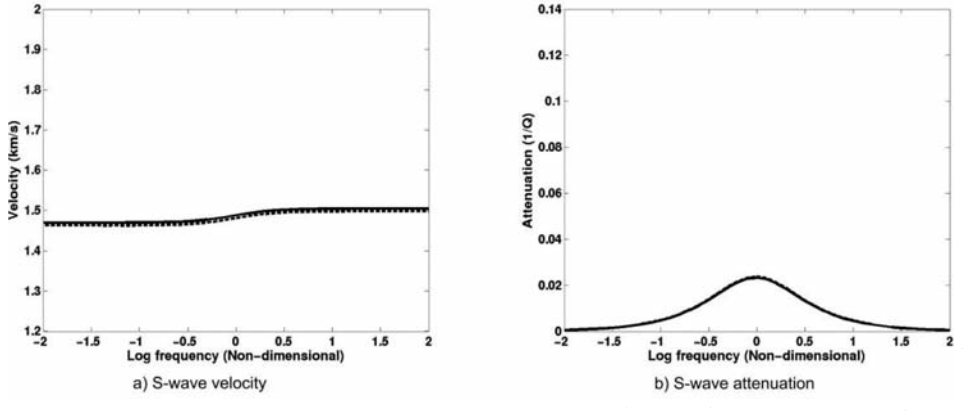

Fig. 1b. Predicted S-velocity and attenuation as a function of non-dimensional frequency $\omega\tau$ under gas and water saturation (solid line: gas, dashed line: water) (Chapman et al., 2006).

dependent velocities, which for simplicity are taken real-valued, the reflectivity can be written as

$$R(\theta,f) = A(\theta)R_P(f) + B(\theta)R_S(f) \quad , \tag{1}$$

where θ is the angle of incidence, $A(\theta) = (5/8) - \frac{1}{2}k^2\sin^2\theta + \frac{1}{2}\tan^2\theta$ and $B(\theta) = -4k^2\sin^2\theta$ are known terms in the AVO inversion processing derived using the initial velocity model, where $k = V_S/V_P$ is a constant defined by the velocity ratio. $R_P(f) = (\Delta V_P/V_P)(f)$ and $R_S(f) = (\Delta V_S/V_S)(f)$ are the frequency-dependent P-wave and S-wave reflectivities, respectively. Because the acquired seismic data is band-limited in frequency, with a dominant frequency value, we only use a limited frequency range of seismic trace data for inversion. Using the Taylor series expansion method around a reference frequency component f_0, eq. (1) can be expanded as

$$R(\theta,f) = A(\theta)R_P(f_0) + (f-f_0)A(\theta)D_P + B(\theta)R_S(f_0) + (f-f_0)B(\theta)D_S \quad , \tag{2}$$

where D_P and D_S are the derivatives of the seismic wave velocities with frequency:

$$D_P = dR_P/df \; ; \; D_S = dR_S/df \quad . \tag{3}$$

Eq. (2) can be used to solve for the two parameters in eq. (3) using a conventional AVO inversion method (Smith and Gidlow, 1987) by adding a frequency component to the inversion matrix. Therefore, for prestack migrated common depth point (CDP) gathers with n offsets denoted by the data matrix s(t,n), we can perform time-frequency decomposition on s(t,n) to derive the seismic spectral amplitude dataset S(t,n,f) with a series of frequencies. The coefficients A and B in the equations, denoted at each sampling time point as $A_n(t)$ and $B_n(t)$, can be derived by the ray tracing method using the initial velocity model. Considering m frequencies $[f_1, f_2, \ldots f_m]$, eq. (2) can be expressed in matrix form:

$$\begin{bmatrix} S(t,1,f_1)-A_1(t)R_P(f_0,t)-B_1(t)R_S(f_0,t) \\ \cdots \\ S(t,1,f_m)-A_1(t)R_P(f_0,t)-B_1(t)R_S(f_0,t) \\ \vdots \\ S(t,n,f_1)-A_n(t)R_P(f_0,t)-B_n(t)R_S(f_0,t) \\ \cdots \\ S(t,n,f_m)-A_n(t)R_P(f_0,t)-B_n(t)R_S(f_0,t) \end{bmatrix} = \begin{bmatrix} (f_1-f_0)A_1(t) & (f_1-f_0)B_1(t) \\ \cdots & \cdots \\ (f_m-f_0)A_1(t) & (f_m-f_0)B_1(t) \\ \vdots & \vdots \\ (f_1-f_0)A_n(t) & (f_1-f_0)B_n(t) \\ \cdots & \cdots \\ (f_m-f_0)A_n(t) & (f_m-f_0)B_n(t) \end{bmatrix} \begin{bmatrix} D_P \\ D_S \end{bmatrix} . \tag{4}$$

Set up the vectors **S** and **A** as below:

$$\mathbf{S} = \begin{bmatrix} S(t,1,f_1) - A_1(t)R_P(f_0,t) - B_1(t)R_S(f_0,t) \\ \cdots \\ S(t,1,f_m) - A_1(t)R_P(f_0,t) - B_1(t)R_S(f_0,t) \\ \vdots \\ S(t,n,f_1) - A_n(t)R_P(f_0,t) - B_n(t)R_S(f_0,t) \\ \cdots \\ S(t,n,f_m) - A_n(t)R_P(f_0,t) - B_n(t)R_S(f_0,t) \end{bmatrix}$$

$$\mathbf{A} = \begin{bmatrix} (f_1 - f_0)A_1(t) & (f_1 - f_0)B_1(t) \\ \cdots & \cdots \\ (f_m - f_0)A_1(t) & (f_m - f_0)B_1(t) \\ \vdots & \vdots \\ (f_1 - f_0)A_n(t) & (f_1 - f_0)B_n(t) \\ \cdots & \cdots \\ (f_m - f_0)A_n(t) & (f_m - f_0)B_n(t) \end{bmatrix}$$

$$\mathbf{D} = \begin{bmatrix} D_P \\ \\ D_S \end{bmatrix} .$$

Then, we can obtain the equation as follows:

$$\mathbf{S} = \mathbf{AD} \quad . \tag{5}$$

The least-squares inversion method can be used to estimate the frequency-dependent attributes D_P and D_S,

$$\mathbf{D} = (\mathbf{A}^T\mathbf{A})^{-1}\mathbf{A}^T\mathbf{S} \quad . \tag{6}$$

An efficient implementation

In our method, we established that an efficient implementation for the FDAI includes gather pre-processing, amplitude balancing and inversion stabilizing in three parts. First, the FDAI method decomposes the prestack seismic gather into a series of frequency components using a time-frequency analysis method. In order to implement FDAI processing using real field seismic data, there are three major processing steps. Step 1: prepare and process the prestack seismic data and perform prestack migration to output the CDP gathers. Step 2: perform time-frequency decomposition on the CDP gathers, analyse the frequency distribution of seismic data, and select the major frequency components for inversion, including low and high frequencies around the dominant frequency. Step 3: perform ray tracing using an initial velocity model to determine the coefficients $A_n(t)$ and $B_n(t)$, and perform FDAI for velocity dispersion using the selected frequency components.

Second, the seismic amplitude spectrum after decomposition must be balanced for the imprint of the seismic wavelet in the trace data before performing FDAI. The aim is to keep the frequency-dependent characteristic in the prestack gather and suppress the wavelet amplitude effect. A suitable weighting function is required in designing an amplitude ratio factor to balance the amplitudes of all frequency components, as the following equation,

$$D(\theta,f) \rightarrow W(\theta,f)D(\theta,f) = S(\theta,f) \quad , \tag{7}$$

where $D(\theta,f)$ is the decomposed seismic data, $W(\theta,f)$ is the weighting function for amplitude balancing, and $S(\theta,f)$ is the balanced seismic frequency dataset. The weighting function for different incident angle gathers can be calculated using the root-mean-square amplitude over a time window.

Finally, according to the numerical modeling results of Chapman et al., (2006), the S-wave velocity dispersion is significantly smaller than the P-wave velocity dispersion (Fig. 1b). For the FDAI inversion calculation, we can simplify the inversion equation by neglecting the S-wave velocity dispersion effect with frequency and stabilizing the inversion processing. Therefore, we can simplify eq. (2) by neglecting the shear-wave velocity first order derivative as follows:

$$R(\theta,f) = A(\theta)R_P(f_0) + (f - f_0)A(\theta)D_P + B(\theta)R_S(f_0) \quad . \tag{8}$$

Further, the FDAI inversion matrix can be written as:

$$\begin{bmatrix} S(t,1,f_1)-A_1(t)R_P(f_0,t)-B_1(t)R_S(f_0,t) \\ \cdots \\ S(t,1,f_m)-A_1(t)R_P(f_0,t)-B_1(t)R_S(f_0,t) \\ \vdots \\ S(t,n,f_1)-A_n(t)R_P(f_0,t)-B_n(t)R_S(f_0,t) \\ \cdots \\ S(t,n,f_m)-A_n(t)R_P(f_0,t)-B_n(t)R_S(f_0,t) \end{bmatrix} = \begin{bmatrix} (f_1-f_0)A_1(t) & (f_1-f_0)B_1(t) \\ \cdots & \cdots \\ (f_m-f_0)A_1(t) & (f_m-f_0)B_1(t) \\ \vdots & \vdots \\ (f_1-f_0)A_n(t) & (f_1-f_0)B_n(t) \\ \cdots & \cdots \\ (f_m-f_0)A_n(t) & (f_m-f_0)B_n(t) \end{bmatrix} D_P \quad . \tag{9}$$

Eq. (9) is more suitable and stable for inverting the prestack seismic data than eq. (4).

APPLICATION TO A HYDROCARBON RESERVOIR

The reservoir in the study area is sandstone and the hydrocarbon is oil. For hydrocarbon detection, in application to real field seismic data, our case study involves a well drilled into an amplitude anomaly (see Fig. 4) which encountered a 27% porosity sandstone reservoir encased in shale (see Fig. 2), with 4.0 m thickness of oil layer. Fig. 2 shows the composite well-logs through

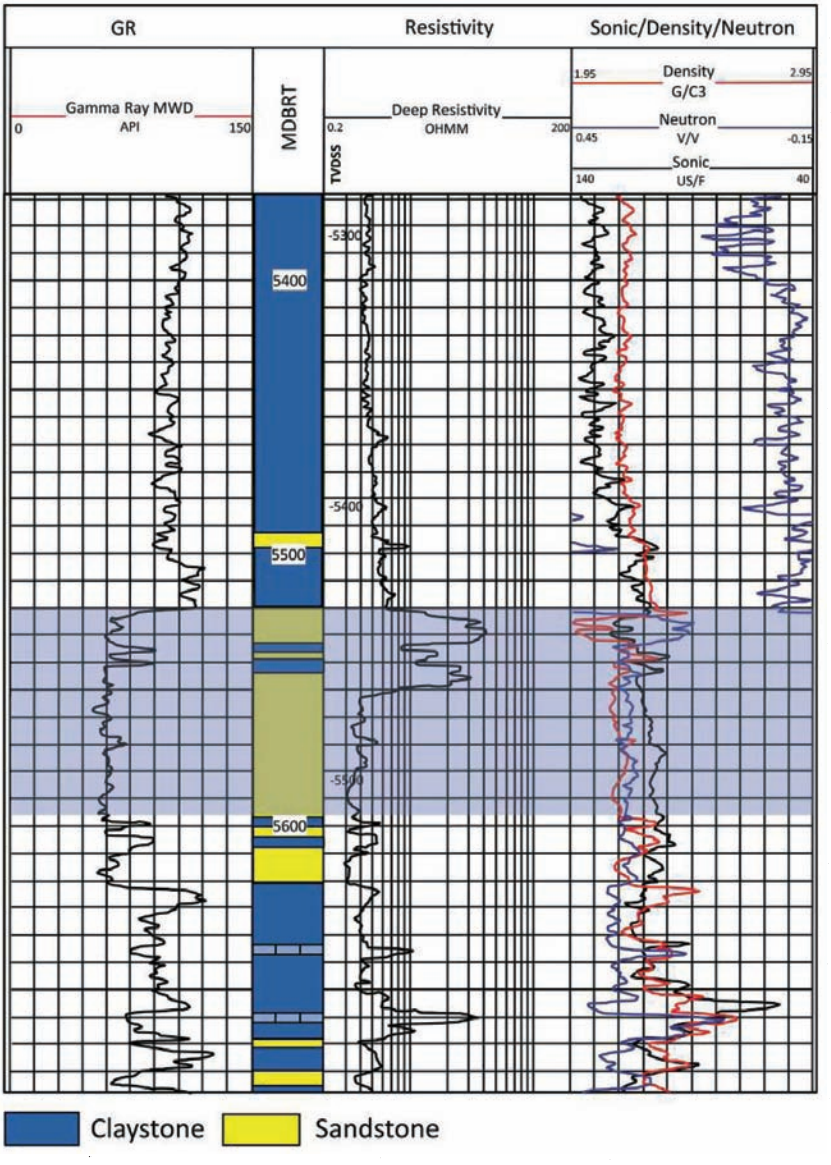

Fig. 2. Composite well log curves through the top of the sandstone reservoir.

the sandstone reservoir, including GR, resistivity, sonic and density curves. The second column shows the lithology, including claystone (blue) and sandstone (yellow). The shading in the figure indicates the sandstone reservoir with lower GR value (in the first column). The hydrocarbon layer is at the top of the reservoir. The deep resistivity curve in the third column shows high resistivity values, and the density curve (the grey line in the fourth column) shows a change to lower values, corresponding to the oil-filled zone.

The seismic reflection response from the hydrocarbon-bearing zone will be clear, due to the distinct change in parameters (shown in figure 2) in the oil sandstone reservoir corresponding to the enclosing claystone. Fig. 3 shows the prestack time-migrated CDP gathers across the drilled well, where the black line in the figure indicates the well location. Although the hydrocarbon-bearing zone is relatively thin, the gathers do indicate a noticeable increase in amplitude with offset (about time 1.67 s). The blue rectangle indicates the reflection response with a Class III AVO characteristic. The strong amplitude is evident at the far offsets (Fig. 4). In Fig. 4, the line is the drilled well location and the circle shows the seismic anomaly of the hydrocarbon reservoir.

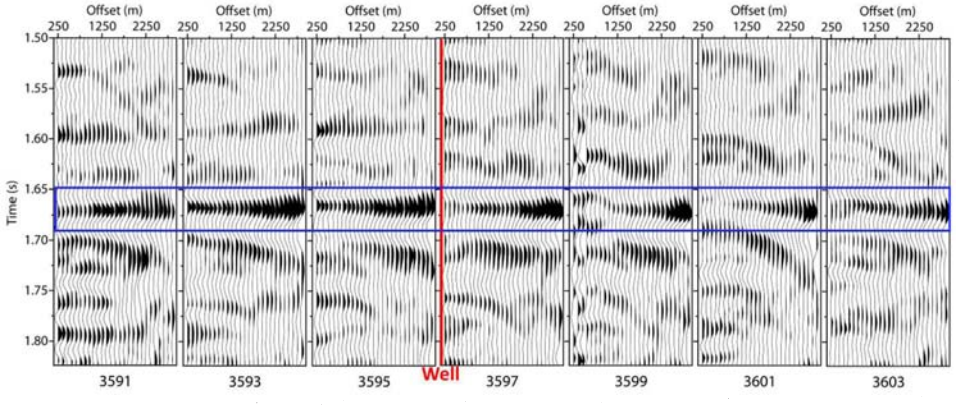

Fig. 3. Prestack time migrated CDP gathers across the well location at times from 1.5 to 1.82 s. The sandstone reservoir response locates at about 1.67 s (rectangle); the CDP numbers are 3591, 3593, 3595, 3597, 3599, 3601 and 3603, respectively, and the drilled well is at CDP 3597 (black line).

Here, we compare the near offset stack section to the far offset stack section. The former has a comparable amplitude response around the drilled well location to the other sandstone. However, the notable "bright point" amplitude shows clearly for the latter.

For the application of the FDAI method to the real field dataset, starting from conventional AVO analysis and modeling, we achieved the frequency-dependent AVO inversion result using our proposed method. The gradient and intercept cross-plot and AVO parameter sections are the most popular means of reservoir characterization. In this study, we also calculated AVO attributes which can be used to validate the FDAI inversion result.

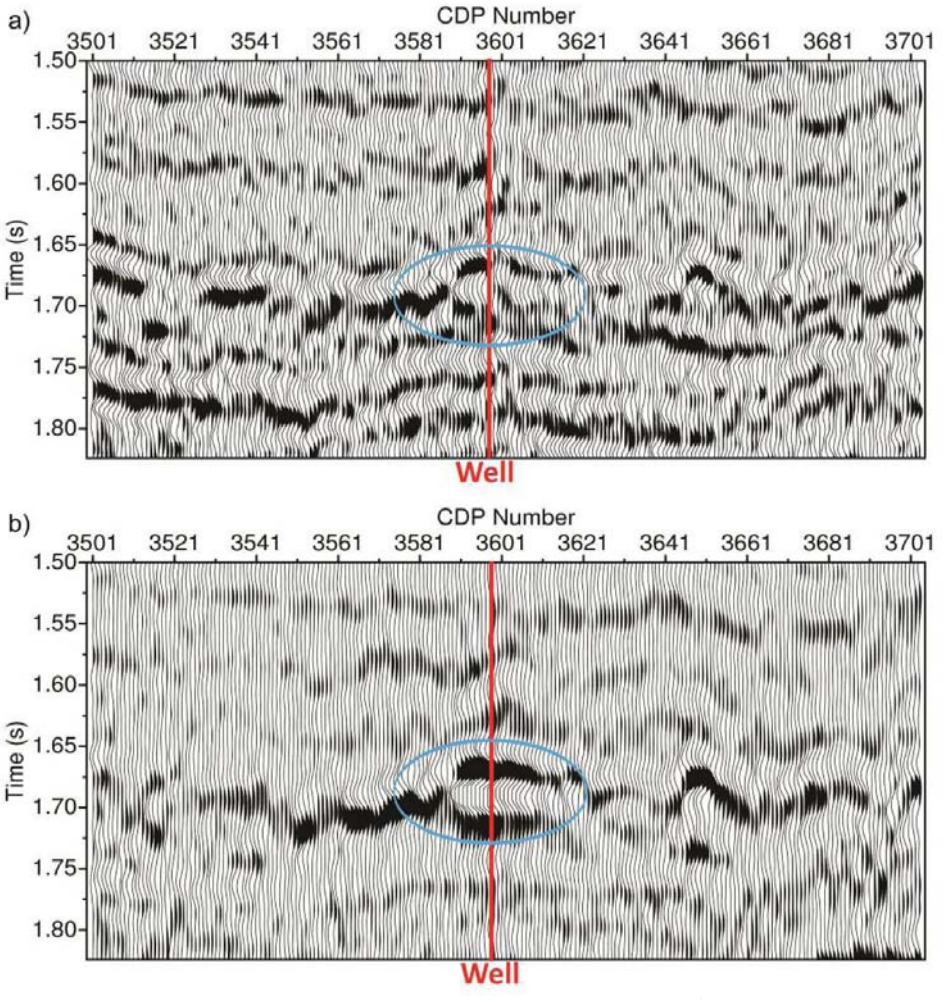

Fig. 4. Comparison of near- and far-offset stacked sections: (a) the near offset stacked section using the prestack time migrated CDP gather between the 250 m and 1250 m range of offsets; (b) the far offset stacked section using the prestack time migrated CDP gather between the 1250 m and 2750 m range of offsets.

Fig. 5 is a cross-plot of the gradient and intercepts which shows a somewhat complex AVO response. There is, however, a discrete Class III type AVO anomaly (red ellipse, hydrocarbon response) that coincides with the thin hydrocarbon zone. In the figure, the bar on the right gives the time of seismic response, and the points in the ellipse are from the hydrocarbon zone. After AVO analysis, the AVO attribute section can be calculated from the prestack gathers. Here, we calculated two AVO attributes (scaled Poisson's ratio and polarization magnitude), which are shown in Fig. 6, overlaid by a P-wave impedance well-log (red line). The scaled Poisson's ratio is defined as $aA+bB$,

where A is the AVO intercept, B is the AVO gradient, a and b are scale parameters, here a = b = 0.5. This is a traditional AVO parameter for identifying an anomaly due to hydrocarbon from the shale background trend. Fig. 6a shows the clear AVO response around the oil-bearing zone. An alternative approach to identifying AVO anomalies is to consider AVO polarization in the intercept-gradient plane. The benefit of the polarization attribute method is that the wavelet is taken into consideration as it is convolved with the reflection coefficients (Keho et al., 2001). Fig. 6b shows the polarization magnitude, defined as the length of the polarization vector, which also reveals the AVO anomalies of the oil-bearing zone. Considering the wavelet in polarization parameters, the AVO anomalies have lower resolution for identifying hydrocarbon than the scaled Poisson's ratio attribute.

Based on the composite well-logs, the AVO characteristic and frequency-dependent behavior of the reservoir can be modeled using a sandwich model of shale and sandstone. The P-wave velocity (α), S-wave velocity (β) and density (ρ) parameters are extracted from the composite well-log curves (Fig.2). In the model, these parameters are 2344.6 m/s, 849 m/s and 2.16 g/cc respectively in the cap rock, and 2822.2 m/s, 1260 m/s and 2.15 g/cc in the sand reservoir. Using the model parameters, we computed the AVO response curves as shown in Fig. 7a. In the figure, the grey line is the simplified Aki equation (Aki and Richards, 1980) for total reflectivity with incident angle, which reveals the same class III AVO response to the prestack seismic gathers

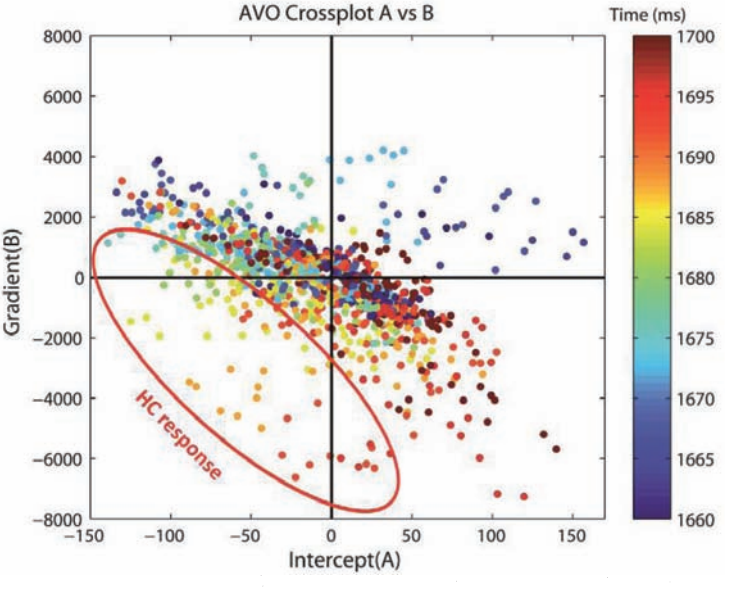

Fig. 5. AVO cross plot for well. The circle indicates the hydrocarbon response (HC). The points correspond to the times indicated by the bar.

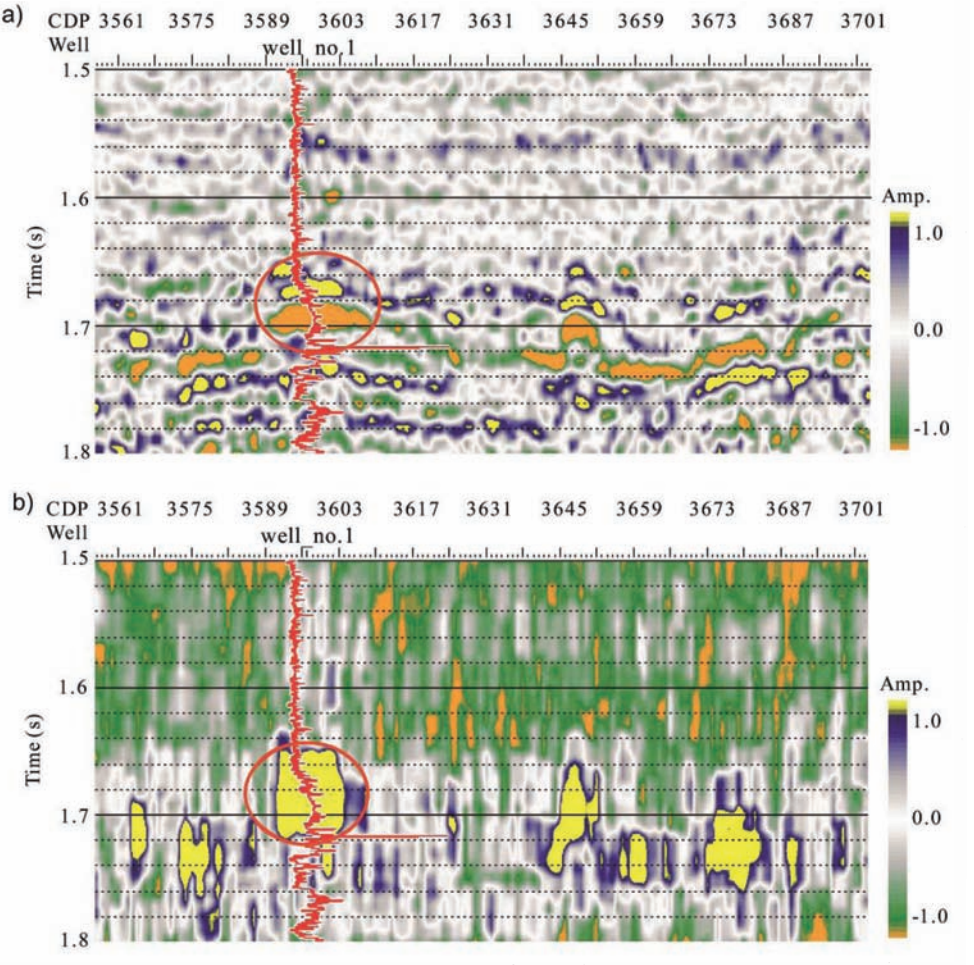

Fig. 6. AVO attributes of (a) Scaled Poisson's ratio change (aA + bB), where a and b are scale parameters, A is the AVO intercept, B is the AVO gradient. (b) Polarization magnitude. The red well-log traces are P-wave impedance. The red circle indicates the AVO anomaly induced by hydrocarbon.

(see Fig. 3), and the black dot, solid and dashed lines are the density (ρ), P-wave velocity (α) and S-wave velocity (β) contributions to the total reflectivity, respectively [eq. (A-7)]. The shear-velocity is the main contribution to the AVO characteristic. Using the cap rock and reservoir sandstone parameters, we established a two-layer Class III AVO model, where the upper layer is elastic and the lower layer is a dispersive medium. Modeling results for

the elastic model and frequency-dependent model of the reservoir are shown in Figs. 7b and 7c, respectively. For the dispersive modeling case, we modeled fluid substitution for water and oil saturation by changing the fluid bulk modulus. For the elastic modeling, the P- and S-wave velocities of the reservoir

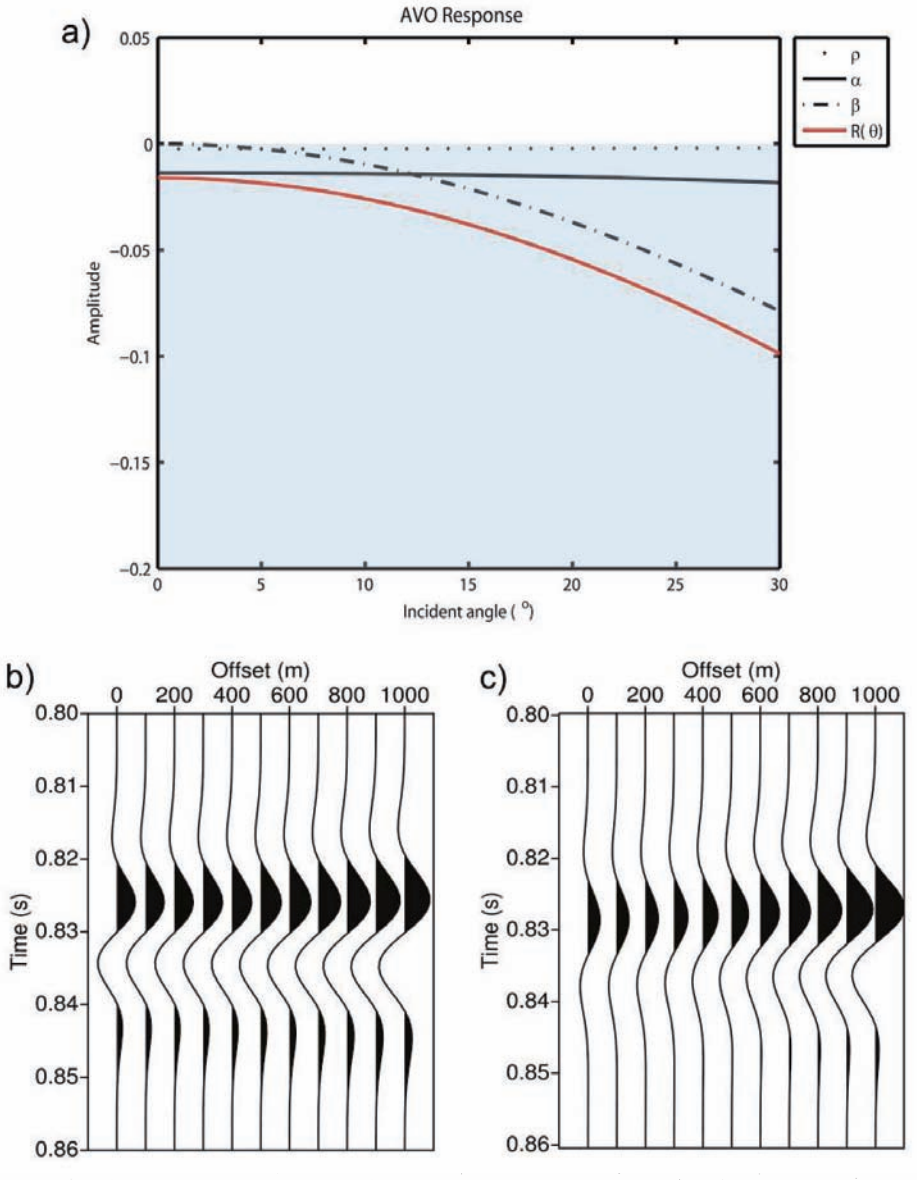

Fig. 7. Comparison of AVO modeling curves. (a) AVO curve indicates class III response; (b) AVO modeling using elastic method; (c) AVO modeling using frequency-dependent method (Chapman et al., 2006).

layer were calculated using the low frequency limit. The whole offset length of modeling is 1000 m, with eleven traces at 100 m intervals. The synthetic seismic wavelet source is a 40 Hz Ricker wavelet. The synthetic gathers are corrected using the exact velocity in NMO processing, and in both cases the amplitudes increase gradually with offset revealing the class III AVO response. Compared to the real field gathers in Fig. 3, the characteristic of the dispersive model is much more consistent than the elastic model to the reflection event at 0.82 s and 0.83 s in Figs. 7b and 7c. Therefore, based on the modeling results, the dispersive characteristic of the real field seismic gathers exists in the hydrocarbon bearing zone, which can be inverted using the proposed FDAI method.

Through the AVO attributes analysis and the dispersive AVO modeling, the AVO anomalies and the frequency-dependent characteristic have been verified in the seismic dataset, corresponding to the hydrocarbon-bearing zone. So, we can use this seismic dataset to invert the frequency-dependent anomalies resulting from the reservoir to verify the proposed FDAI method. As the input of FDAI is the different prestack frequency gathers, the first procedure is to decompose the gathers in the time-frequency domain to obtain the frequency component, using a time-frequency decomposition method. Fig. 8 shows the time-frequency decomposed CDP gathers at the different iso-frequencies, covering the same ranges as in Fig. 3. In Fig. 8, we show two CDP ranges for comparison of the frequency-dependent characteristic. Fig. 8a corresponds to the hydrocarbon-bearing range, in which the CDPs are from 3591 to 3603 crossing the drilled well location (CDP 3597). Fig. 8b is outside the oil zone in which the CDPs are from 3529 to 3541 (see the stacked section in Fig. 4b and AVO attribute sections in Fig. 6). The former reveals frequency variations in the high frequency range which relate to the dispersive hydrocarbon zone. The latter has a greater high frequency component which reveals the less dispersive response. For the FDAI, we choose four frequency components to invert - 10 Hz, 20 Hz, 40 Hz and 60 Hz, which cover the seismic data frequency band range. Finally, using the prestack frequency gathers shown in Fig. 8 as the input to the FDAI method, we invert the P-wave velocity dispersion. Fig. 9 shows the results of FDAI applied to the data in Fig. 8, and the distribution of the hydrocarbons is clearly represented by the high dispersion anomaly within the hydrocarbon zone, denoted by the solid white circle and a well-log curve. The P-wave velocity dispersion was inverted using the FDAI method, which indicates that the frequency-dependent wave dispersion results from fluid flow in porous media (the oil-bearing zone in the reservoir). The dashed white circle indicates a separated high dispersion anomaly which may be a hydrocarbon zone. These anomalies can be verified by the AVO attribute sections in Fig. 6. Moreover, the FDAI inverted results show significant dispersive anomalies that degrade the elastic characteristic which can be found in the traditional AVO attribute sections. It means that the FDAI method has a much better capability for hydrocarbon detection, using the frequency-dependent response in the reservoir.

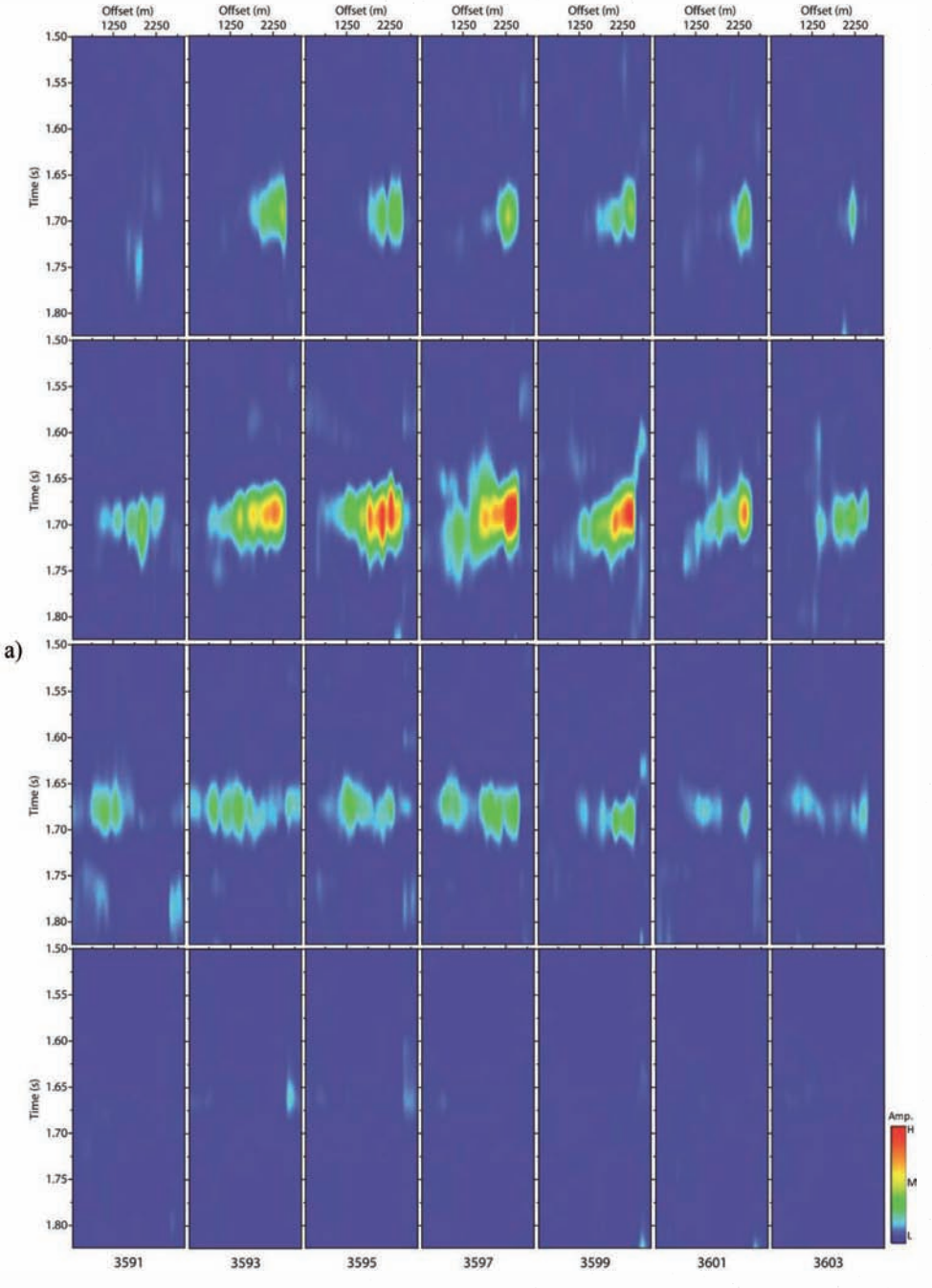

Fig. 8. (a) Spectral amplitudes of the decomposed prestack CDP gathers, **in** the hydrocarbon zone using the time-frequency analysis method at four different iso-frequencies 10 Hz, 20 Hz, 40 Hz and 60 Hz (top to bottom panels).

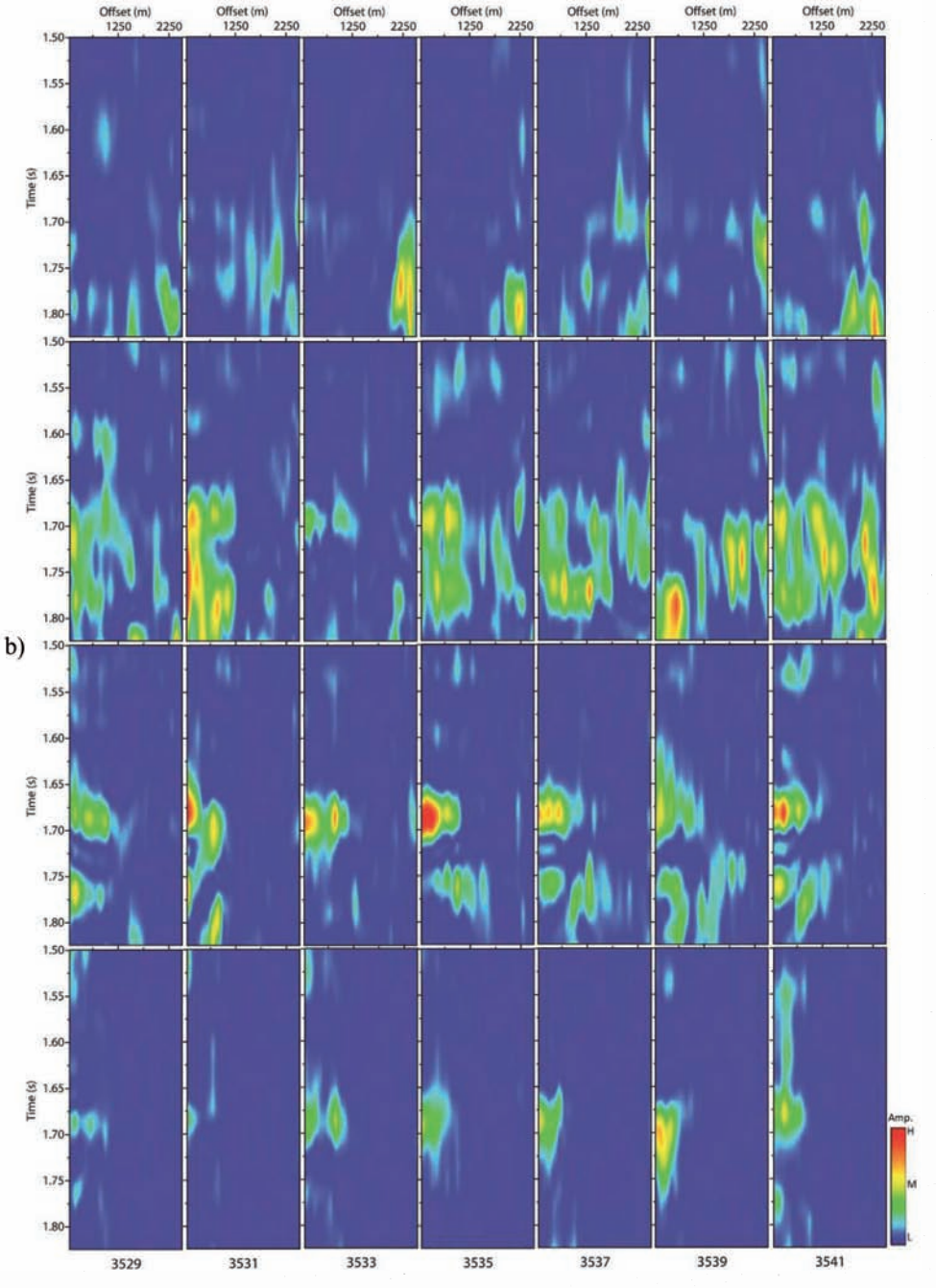

Fig. 8. (b) Spectral amplitudes of the decomposed prestack CDP gathers, **out** of the hydrocarbon zone using the time-frequency analysis method at four different iso-frequencies 10 Hz, 20 Hz, 40 Hz and 60 Hz (top to bottom panels).

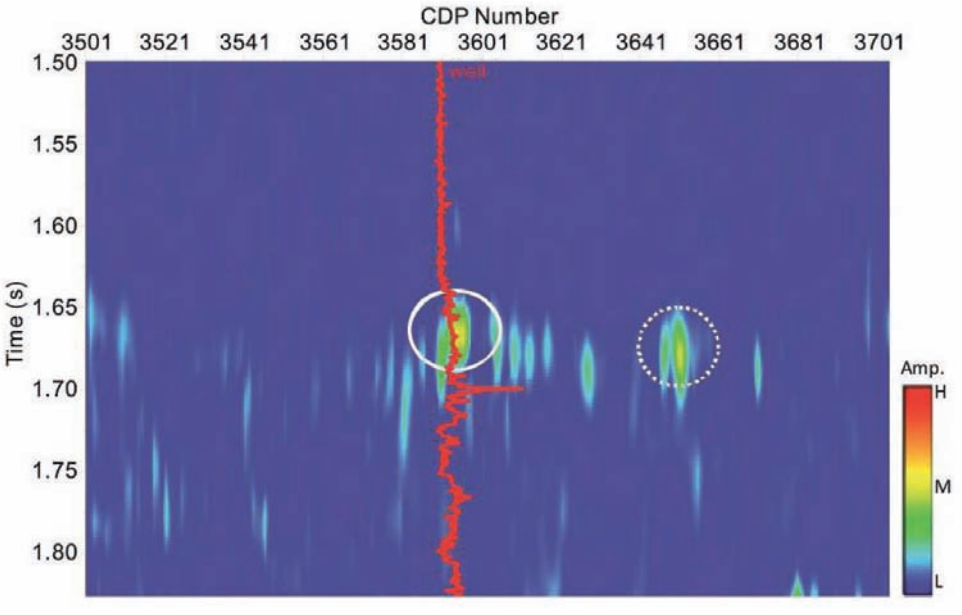

Fig. 9. P-wave velocity dispersion anomaly obtained by FDAI, correlated with the distribution of hydrocarbons. The white circle is the range of the oil-bearing reservoir with warm colours indicating high dispersion values matching fluid distribution in the sand reservoir.

DISCUSSION AND CONCLUSIONS

In this paper, we have proposed a frequency-dependent AVO inversion method for the velocity dispersion of wave-induced fluid flow in a hydrocarbon reservoir and applied it to a real field seismic dataset. Our main goal was to devise a frequency-dependent AVO inversion approach, based on the squirt-flow mechanism, that not only inverts the seismic wave velocity dispersion characteristic (the frequency-dependent reflection coefficient of the reflected

reservoirs resulting in a frequency-dependent characteristic. The limited squirt-flow mechanism of this study does not allow us to make the same statement for the other frequency-dependent responses.

For the scale-dependent interface, there are the frequency-dependent characteristics of the reflection and transmission coefficients (Wapenaar, 1998; Wapenaar et al., 1999, 2004). Herrmann (1997) investigated the character of the outliers in well-logs by using a multiscale singularity detection approach as proposed by Mallat and Hwang (1992). This frequency-dependent characteristic has a different mechanism to the velocity dispersion resulting from wave-induced fluid flow in reservoir. Scale-dependent velocity induced reflection coefficient variations do not have a clear relation with the hydrocarbons in a reservoir, though they are frequency-dependent. The squirt-flow mechanism of wave-induced fluid flow has been verified by the test of cores in a laboratory (Baztle et al., 2006) and numerical modeling (Chapman et al., 2006), which is the main theory behind the use of the frequency-dependent characteristic for hydrocarbon detection.

NMO stretch occurs when the normal moveout correction widens a wavelet's period, which amplifies the low frequencies and reduces the high frequencies (Xu and Chopra, 2007) and affects the frequency-dependent characteristic. It will increase the tuning bed thicknesses and reduce the resolution, and must be corrected before making tuning bed corrections. Though it has a similar effect on the frequency spectra, it is different from frequency-dependent AVO, in which wave-induced fluid flow occurs in rock. And it also increases with offset, since the signal has more rock to pass through. Unlike NMO stretch, the frequency-dependent AVO depends not only on offset but also on the petrophysical characteristics of the rocks the seismic wave passes through.

In conclusion, wave-induced fluid flow in hydrocarbon reservoirs results in frequency-dependent reflection coefficients for the prestack seismic gathers, resulting in a frequency-dependent AVO response, which can help to further invert for the velocity dispersion characteristic and be used to detect hydrocarbons. The proposed inversion method (FDAI) has been tested using field seismic data. The method has been verified through application to a known hydrocarbon bearing reservoir zone, and we find that the inversion method is stable and suitable for prestack seismic inversion. The field seismic example indicates the potential of the FDAI method for the detection of seismic wave velocity dispersion. In the application to field seismic data, we observed significant changes of seismic wave dispersion. The inversion results indicate that seismic wave attenuation and dispersion can be detected quantitatively using the frequency dependent inversion method, and in particular, attenuation and dispersion characteristics resulting from wave-induced fluid flow in porous media can be quantified.

ACKNOWLEDGEMENTS

This work is sponsored by the National Science & Technology Major Project (Grant No. 2011ZX05019-008), supported by PetroChina Innovation Foundation (Grant No. 2012D-5006-0301) and the Science Foundation of China University of Petroleum-Beijing (Grant No. KYJJ2012-05-11), and is to be published with the permission of the EAP sponsors and the Executive Director of the British Geological Survey (NERC). The authors would also like to thank the anonymous reviewers for their constructive comments on the manuscript, and David Booth for proof reading the manuscript.

REFERENCES

Arntsen, B. and Carcione, J.M., 2001. Numerical simulation of the Biot slow wave in water-saturated Nivelsteiner sandstone. Geophysics, 66: 890-896.

Aki, K. and Richards, P.G., 1980. Quantitative Seismology, Theory and Methods, Vol. 1. W.H. Freeman and Co., San Francisco.

Batzle, M., Hofmann, R., Han, D. and Castagna, J., 2001. Fluid sand frequency dependent seismic velocity of rocks. The Leading Edge, 20: 168-171.

Batzle, M., Han, L.D. and Hofmann, R., 2006. Fluid mobility and frequency-dependent seismic velocity-direct measurements. Geophysics, 71: N1-N9.

Biot, M.A., 1956a. Theory of propagation of elastic waves in fluid-saturated porous solid. I. Low-frequency range. J. Acoust. Soc. Am., 28: 168-178.

Biot, M.A., 1956b. Theory of propagation of elastic waves in a fluid-saturated porous solid. II. Higher frequency range. J. Acoust. Soc. Am., 28: 179-191.

Biot, M.A., 1962. Mechanics of deformation and acoustic propagation in porous media. J. Appl. Phys., 33: 1482-1498.

Carcione, J.M., 2001. Wave Fields in Real Media: Wave Propagation in Anisotropic, Anelastic and Porous Media. Pergamon Press, Oxford.

Carcione, J.M. and Picotti, S., 2006. P-wave seismic attenuation by slow wave diffusion: Effects of inhomogeneous rock properties. Geophysics, 71: 1-8.

Castagna, J.P., Sun, S. and Siegfried, R.W., 2003. Instantaneous spectral analysis: detection of low-frequency shadows associated with hydrocarbons. The Leading Edge, 22: 120-127.

Chapman, M., 2003. Frequency dependent anisotropy due to mesoscale fractures in the presence of equant porosity. Geophys. Prosp., 51: 369-379.

Chapman, M., Lin, E. and Li, X.-Y., 2006. The influence of fluid-sensitive dispersion and attenuation on AVO analysis. Geophys. J. Internat., 167: 89-105.

Chen, S.Q., Li, X.-Y. and Wang, S.X., 2012. The analysis of frequency-dependent characteristics for fluid detection: a physical model experiment. Appl. Geophys., 9: 195-206.

Dvorkin, J., Mavko, G. and Nur, A., 1995. Squirt flow in fully saturated rocks. Geophysics, 60: 97-107.

Ebrom, D., 2004. The low-frequency gas shadow on seismic sections. The Leading Edge, 23: 772.

Gassmann, F., 1951. Über die Elastizität poroser Medien. Veirteljahrsschr. Naturforsch. Gesellsch. Zürich, 96: 1-23.

Goloshubin, G.M. and Korneev, V.A., 2000. Seismic low-frequency effects from fluid-saturated reservoir. Expanded Abstr., 70th Ann. Internat. SEG Mtg., Calgary: 976-979.

Gurevich, B., Zyrianov, V.B. and Lopatnikov, S.L., 1997. Seismic attenuation in finely layered porous rocks: Effects of fluid flow and scattering. Geophysics, 62: 319-324.

Herrmann, F.J., 1997. A Scaling Media Representation, a Discussion on Well-logs, Fractals and Waves. Ph.D. thesis, Delft University of Technology, Delft.

Innanen, K., 2011. Inversion of the seismic AVF/AVA signatures of highly attenuative targets. Geophysics, 76: R1-R14.

Jakobsen, M. and Chapman, M., 2009. Unified theory of global flow and squirt flow in cracked porous media. Geophysics, 74: WA65-WA76.

Johnson, D.L., 2001. Theory of frequency dependent acoustics in patchy saturated porous media. J. Acoust. Soc. Am., 110: 682-694.

Keho, T., Lemanski, S., Ripple, R. and Tambunan, B., 2001. The AVO hodogram: Using polarization to identify anomalies. The Leading Edge, 20: 1214-1224.

Korneev, V.A., Goloshubin, G.M., Daley, T.M. and Silin, D.B., 2004. Seismic low-frequency effects in monitoring fluid-saturated reservoirs. Geophysics, 69: 522-532.

Li, X.-Y. and Zhang, Y., 2011. Seismic reservoir characterization: How can multicomponent data help? J. Geophys. Engin., 8: 123-141.

Liner, C.L., Bell, L. and Verm, R., 2009. Direct imaging of group velocity dispersion curves in shallow water. Expanded Abstr., 79th Ann. Internat. SEG Mtg., Houston: 3317-3321.

Liu, E., Queen, J.H., Li, X.Y., Maultzsch, M.S., Lynn, H.B. and Chesnokov, E.M., 2003. Observation and analysis of frequency-dependent anisotropy from a multicomponent VSP at Bluebell-Altamont field, Utah. J. Appl. Geophys., 54: 319-333.

Liu, E., Chapman, M., Loizou, N. and Li, X., 2006. Applications of spectral decomposition for AVO analyses in the west of Shetland. Expanded Abstr., 76th Ann. Internat. SEG Mtg., New Orleans: 279-283.

Liu, L.F., Cao, S.Y. and Wang, L., 2011. Poroelastic analysis of frequency-dependent amplitude-versus-offset variations. Geophysics, 76: C31-C40.

Mallat, S.G. and Hwang, W.L., 1992. Singularity detection and processing with wavelets. IEEE Trans. Inform. Theory, 38: 617-643.

Marmalyevsky, N. and Roganov, Y., 2006. Frequency depending AVO for a gas-saturated periodical thin-layered stack. Expanded Abstr., 76th Ann. Internat. SEG Mtg., New Orleans: 274-278.

Mochizuki, S., 1982. Attenuation in partially saturated rocks. J. Geophys. Res., 87: 8598-8604.

Müller, T.M. and Gurevich, B., 2004. One-dimensional random patchy saturation model for velocity and attenuation in porous rocks. Geophysics, 69: 1166-1172.

Odebeatu, E., Zhang, Z., Chapman, M., Liu, E. and Li, X-Y., 2006. Application of spectral decomposition to detection of dispersion anomalies associated with gas saturation. The Leading Edge, 25: 206-210.

Parra, J.O., 2000. Poroelastic model to relate seismic wave attenuation and dispersion to permeability anisotropy. Geophysics, 65: 202-210.

Pride, S.R., Berryman, J.G. and Harris, J.M., 2004. Seismic attenuation due to wave induced flow. J. Geophys. Res., 109 (B1): B01201.

Ren, H., Goloshubin, G. and Hilterman, F.J. 2008. Amplitude-versus-frequency variations in thinly layered porous rocks. Expanded Abstr., 78th Ann. Internat. SEG Mtg., Las Vegas: 1744-1746.

Ren, H., Goloshubin, G. and Hilterman, F.J., 2009. Poroelastic analysis of amplitude-versus-frequency variations. Geophysics, 74: O1-O8.

Shapiro, S.A. and Müller, T.M., 1999. Seismic signatures of permeability in heterogeneous porous media. Geophysics, 64: 99-103.

Shuey, R., 1985. A simplification of the Zoeppritz equations. Geophysics, 50: 609-614.

Smith, G.C. and Gidlow, P.M., 1987. Weighted stacking for rock property estimation and detection of gas. Geophys. Prosp., 35: 993-1014.

Wapenaar, C.P.A., 1998. Seismic reflection and transmission coefficients of a self-similar interface. Geophys. J. Internat., 135: 585-594.

Wapenaar, C.P.A., van Wijngaarden, A., van Geloven, W. and van der Leij, T., 1999. Apparent AVA effects of fine layering. Geophysics, 64: 1939-1948.

Wapenaar ,C.P.A., Thorbecke, J. and Draganov, D., 2004. Relations between reflection and transmission responses of three-dimensional inhomogeneous media. Geophys. J. Internat., 156: 179-194.

White., J.E., 1975. Computed seismic speed sand attenuation in rocks with partial gas saturation. Geophysics, 40: 224-232.

White, J.E., 1986. Underground Sound: Applications of Seismic Waves. Geophysical Press Ltd., Amsterdam.

White, J.E., Mikhaylova, G. and Lyakhovitskiy, F.M., 1975. Low-frequency seismic waves in fluid-saturated layered rocks. Izvestija (Russian Academy of Sciences), Phys. Solid Earth, 11: 654-659.

Wilson, A., Chapman, M. and Li, X.-Y., 2009. Frequency-dependent AVO inversion. Expanded Abstr., 79th Ann. Internat. SEG Mtg., Houston, 28: 341-345.

Wolf, A., 1937. The reflection of elastic waves from transition layers of variable velocity. Geophysics, 2: 357-363.

Wu, X., Chapman, M., Wilson, A. and Li, X.-Y., 2010. Estimating seismic dispersion from pre-stack data using frequency-dependent AVO inversion. Expanded Abstr., 80th Ann. Internat. SEG Mtg., Denver, 29: 341-345.

Wu, X., Chapman, M. and Li, X.-Y., 2012. Frequency-dependent AVO attribute: Theory and example. First Break, 30: 67-72.

Xu, D., Wang, Y., Gan, Q. and Tang, J., 2011. Frequency-dependent seismic reflection coefficient for discriminating gas reservoirs. J. Geophys. Engin., 8: 508.

Xu, Y. and Chopra, S., 2007. Improving AVO fidelity by NMO stretching and offset-dependent tuning corrections. The Leading Edge, 26: 1548-1551.

Yoo, S. and Gibson, R.L., 2005. Frequency dependent AVO analysis after target oriented stretch correction. Expanded Abstr., 75th Ann. Internat. SEG Mtg., Houston, 24: 293-296.

Zhang, S., Yin, X. and Zhang, G., 2011. Dispersion-dependent attribute and application in hydrocarbon detection. J. Geophys. Engin., 8: 498-507.

APPENDIX

FREQUENCY-DEPENDENT AVO REFLECTION EQUATIONS

Liu et al. (2011) derived the frequency-dependent reflectivity Zoeppritz equations based on a plane P-wave incident on an interface between homogeneous, isotropic and attenuation media in the x-z plane. It is expressed as

$$\begin{pmatrix} \sin\theta_{P1} & \cos\theta_{S1} & -\sin\theta_{P2} & \cos\theta_{S2} \\ \cos\theta_{P1} & -\sin\theta_{S1} & \cos\theta_{P2} & \sin\theta_{S2} \\ \dfrac{\rho_1 c_{S1}^2}{c_{P1}}\sin 2\theta_{P1} & \rho_1 c_{S1}\cos 2\theta_{S1} & \dfrac{\rho_2 c_{S2}^2}{c_{P2}}\sin 2\theta_{P2} & -\rho_2 c_{S2}\cos 2\theta_{S2} \\ \rho_1 c_{P1}\cos 2\theta_{S1} & -\rho_1 c_{S1}\cos 2\theta_{S1} & -\rho_2 c_{P2}\cos 2\theta_{S2} & -\rho_2 c_{S2}\sin 2\theta_{S2} \end{pmatrix} \times \begin{pmatrix} R_{PP}^* \\ R_{PS}^* \\ T_{PP}^* \\ T_{PS}^* \end{pmatrix} = \begin{pmatrix} -\sin\theta_{P1} \\ \cos\theta_{P1} \\ \dfrac{\rho_1 c_{S1}^2}{c_{P1}}\sin 2\theta_{P1} \\ -\rho_1 c_{P1}\cos 2\theta_{S1} \end{pmatrix}, \quad \text{(A-1)}$$

where c is a frequency-dependent velocity, subscripts P and S represent the P- and S-wave, respectively, subscripts 1 and 2 are the upper and lower media, and

$$1/c_P = [1/V_P(\omega)] - [i\alpha_P(\omega)/\omega] \ , \ 1/c_S = [1/V_S(\omega)] - [i\alpha_S(\omega)/\omega] \ , \quad \text{(A-2)}$$

where ω is the angular frequency, V and α are phase velocity and attenuation coefficient (Carcione, 2001),

$$\alpha = [\sqrt{(Q^2+1)} - Q](\omega/V) \ . \quad \text{(A-3)}$$

θ_{P1} is the P-wave incident angle which is equal to the P-wave reflective angle; θ_{S1} is the converted S-wave reflected angle; θ_{P2} and θ_{S2} are the angles of the transmitted P-wave and S-wave, respectively.

If the velocity does not suffer dispersion, the conventional simplified reflection coefficient from the Zoeppritz equation is (Aki and Richards, 1980)

$$R_{PP}(\theta) = \tfrac{1}{2}(1 - 4k^2\sin^2\theta)(\Delta\rho/\rho) + \tfrac{1}{2}\sec^2\theta(\Delta V_P/V_P) - 4k^2\sin^2\theta(\Delta V_S/V_S) \ , \quad \text{(A-4)}$$

where, V_P and V_S are P- and S-wave velocities, respectively. According to the real part of velocities in eq. (A-2), the analogy expression with the frequency-dependent velocities can be written as

$$R^*_{PP}(\theta,\omega) \approx \tfrac{1}{2}(1 - 4k^2\sin^2\theta)(\Delta\rho/\rho) + \tfrac{1}{2}\sec^2\theta(\Delta V_P/V_P)(\omega) - 4k^2\sin^2\theta(\Delta V_S/V_S)(\omega) \ , \quad \text{(A-5)}$$

where the angular frequency variable $\omega = 2\pi f$. Here, we consider the velocities are frequency-dependent, rather than considering the complex-valued velocities. Solving the exact complex-valued equations is complicated, and beyond the scope of this paper.

Further, taking the density and P-wave velocity to be related by the Gardner function $\rho = mc^{1/4}$ (Gardner et al.,, 1974), where m is a scale constant, we can get a simplified equation containing two parameters without the density term:

$$R^*_{PP}(\theta,\omega) = A(\theta)(\Delta\rho/\rho)(\omega) + B(\theta)(\Delta V_P/V_P)(\omega) \ , \quad \text{(A-6)}$$

where

$$A(\theta) = (5/8) - \tfrac{1}{2}k^2\sin^2\theta + \tfrac{1}{2}\tan^2\theta \ ,$$

and

$$B(\theta) = -4k^2\sin^2\theta \ .$$